Science Advances
AAAS

Supplementary Materials for

Ultrahigh strength, modulus, and conductivity of graphitic fibers by macromolecular coalescence

Dongju Lee, Seo Gyun Kim, Seungki Hong, Cristina Madrona, Yuna Oh, Min Park, Natsumi Komatsu, Lauren W. Taylor, Bongjin Chung, Jungwon Kim, Jun Yeon Hwang, Jaesang Yu, Dong Su Lee, Hyeon Su Jeong, Nam Ho You, Nam Dong Kim, Dae-Yoon Kim, Heon Sang Lee, Kun-Hong Lee, Junichiro Kono, Geoff Wehmeyer, Matteo Pasquali, Juan J. Vilatela*, Seongwoo Ryu*, Bon-Cheol Ku*

*Corresponding author. Email: juanjose.vilatela@imdea.org (J.J.V.); ryu@suwon.ac.kr (S.R.); cnt@kist.re.kr (B.-C.K.)

Published 22 April 2022, *Sci. Adv.* **8**, eabn0939 (2022)
DOI: 10.1126/sciadv.abn0939

This PDF file includes:

Science Advances
AAAS

Supplementary Materials for

Ultrahigh strength, modulus, and conductivity of graphitic fibers by macromolecular coalescence

Dongju Lee, Seo Gyun Kim, Seungki Hong, Cristina Madrona, Yuna Oh, Min Park, Natsumi Komatsu, Lauren W. Taylor, Bongjin Chung, Jungwon Kim, Jun Yeon Hwang, Jaesang Yu, Dong Su Lee, Hyeon Su Jeong, Nam Ho You, Nam Dong Kim, Dae-Yoon Kim, Heon Sang Lee, Kun-Hong Lee, Junichiro Kono, Geoff Wehmeyer, Matteo Pasquali, Juan J. Vilatela*, Seongwoo Ryu*, Bon-Cheol Ku*

*Corresponding author. Email: juanjose.vilatela@imdea.org (J.J.V.); ryu@suwon.ac.kr (S.R.); cnt@kist.re.kr (B.-C.K.)

Published 22 April 2022, *Sci. Adv.* **8**, eabn0939 (2022)
DOI: 10.1126/sciadv.abn0939

This PDF file includes:

Supplementary Text

Wet-spun CNT fibers

The mechanical and electrical properties of CNT fibers depend on purity, crystallinity (G/D ratio), and length (aspect ratio, L/d) of CNTs from a material perspective (*7, 30*). The impurities such as residual catalysts in the CNT can interfere with the continuous spinning process due to unstable flow and blocking of the spinneret (*30*). In addition, the residual particles can deteriorate macroscopic properties by acting as defects in CNT fibers. Here, we obtained more than 98% high purity CNTs through 400 °C heat treatment and piranha solution purification (fig. S1a). The G/D ratios of purified CNTs exceeded 50, indicating high crystallinity (fig. S1b) (*30*). At sufficiently high purity and G/D ratio, the tensile strength and electrical conductivity of CNT fibers show a large dependence on the length with $(L/d)^{0.9}$ and $(L/d)^{0.8}$ scaling relationship, respectively (*30*). The viscosity-averaged aspect ratios of SWNT and S·DWNT used in this work were reported to be ~2000 and ~6700, it was measured by capillary breakup extensional rheometry technique (*7, 30, 43*). In this work, the measured tensile strength and electrical conductivity of pristine SWNT and S·DWNT fibers correspond well with the relationship with the reported aspect ratio (Fig. 3 and fig. S9 and S12).

The mechanical and electrical properties of CNT fibers can be optimized by controlling the process variables such as concentration, draw ratio, and flow type of dope (*18*). The mesoscopic properties of CNT fibers in the same CNT depend on the degree of alignment and packing of CNTs, which can be controlled by the spinning process (*18*). The dopes for spinning were prepared in 1-3 wt%. The liquid crystal dopes were extruded by optimized wet-spinning process at draw ratio of 1.6 or higher considered the stability analysis and rheological properties based on Hyper-Spin-Line (HSL) model (*18*).

Heat treatment of CNT fiber

The wet-spun CNT fibers were annealed at 1400, 1700, 2000, 2400, or 2700 °C. The CNTs in fiber evolved with increasing temperature through the coalescence route (Fig. 1 and fig. S2). The average diameter of CNTs was increased by 6-20% in 1700 and 2000 °C-treated SWNT and

S·DWNT fibers, and the larger diameter CNTs were mostly SWNTs (Fig. 1, fig. S2 and S3). The SWNTs with larger diameter have distorted circular structures in the form of ellipses or polygons (Fig. 1 and fig. S2). In addition, the fraction of MIW-CNT and C-CNT structures was observed to be within 10% in 1700 and 2000 °C-treated fibers (Fig. 1 and fig. S2). With progressing annealing, the proportion of SWNTs decreased, and the proportion of DWNTs relatively increased (Fig. 1, fig. S2 and S3). In contrast, structural evolutions were not well observed in DWNT fibers treated with 1400-2000 °C (fig. S2 and S3). From these results, it can be seen that the less thermally stable SWNTs participates in the coalescence route, leading to an increase of diameter and formation of MIW-CNT and C-CNT. In 2400 °C-treated fibers, CNT bundles started to completely unzip into planar structures for both SWNT and DWNT (Fig. 1 and fig. S2). This planar graphitization with AB stacking graphite nano ribbon (GNR) structure was completed at 2700 °C (Fig. 1 and fig. S2).

Mechanical properties of CNT fibers

The tensile strengths of SWNT and DWNT CNT fibers at each temperature of heat treatment were observed by stress-strain curves (fig. S9). The tensile strength of SWNT fibers was improved by about 77% compared to the pristine SWNT fibers from 0.98 GPa to 1.74 GPa by heat treatment at 2000 °C (fig. S9, Table S1 and S2). At higher temperatures than 2000 °C, the tensile strength decreased while the tensile modulus increased as the CNTs changed into graphitic structures. In the case of DWNT fibers, the tensile strength remains similar up to 2000 °C. These results are related to the structural evolutions due to difference in thermal stability between SWNT and DWNT up to 2000 °C (fig. S3).

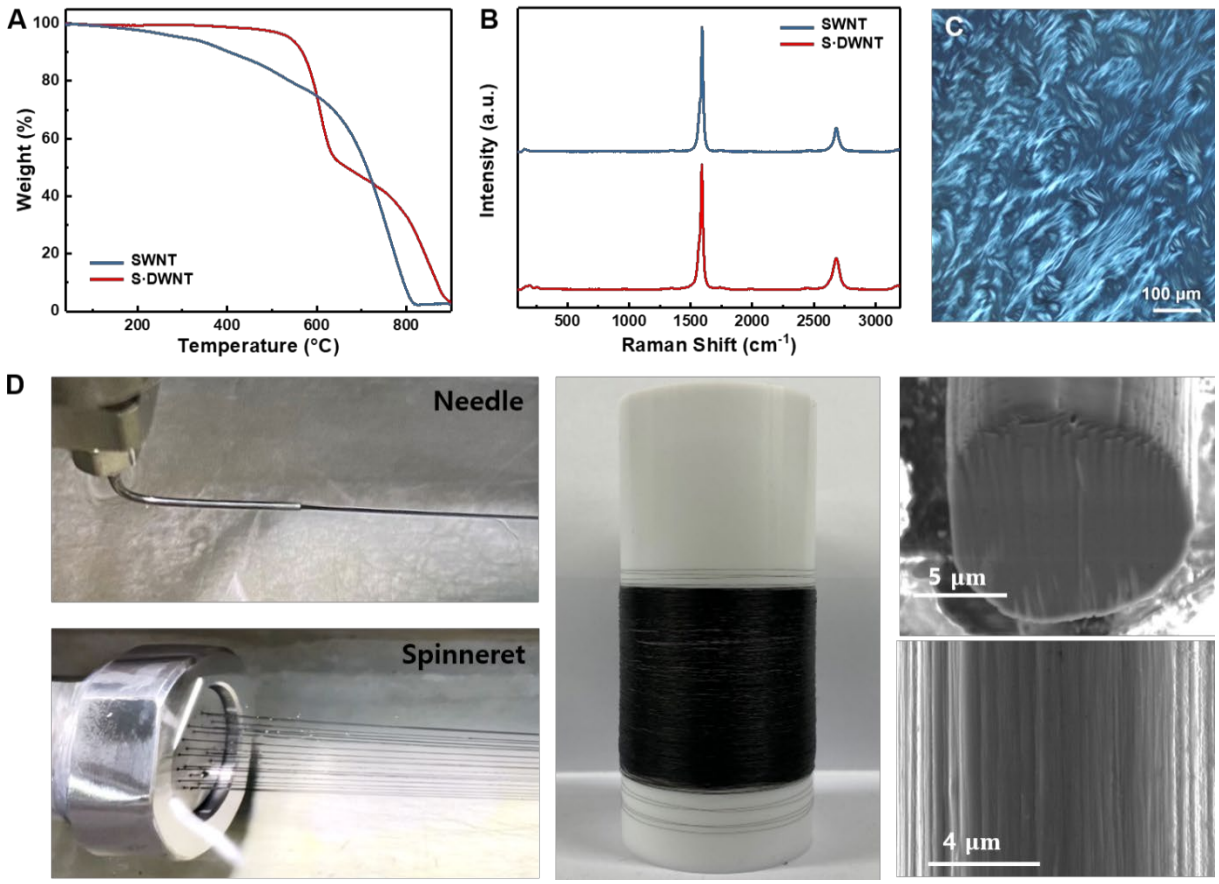

Figure S1. Properties and fabrication process of liquid crystal based CNT fibers. (**A**) TGA and (**B**) Raman analysis of pristine SWNT and S·DWNTs. (**C**) Cross-polarized image of liquid crystal S·DWNT dope (1.0 vol%). (**D**) Wet-spun CNT fibers obtained by needle and 24-holes spinneret through wet-spinning process, and cross-sectional and surface images of as spun CNT fibers.

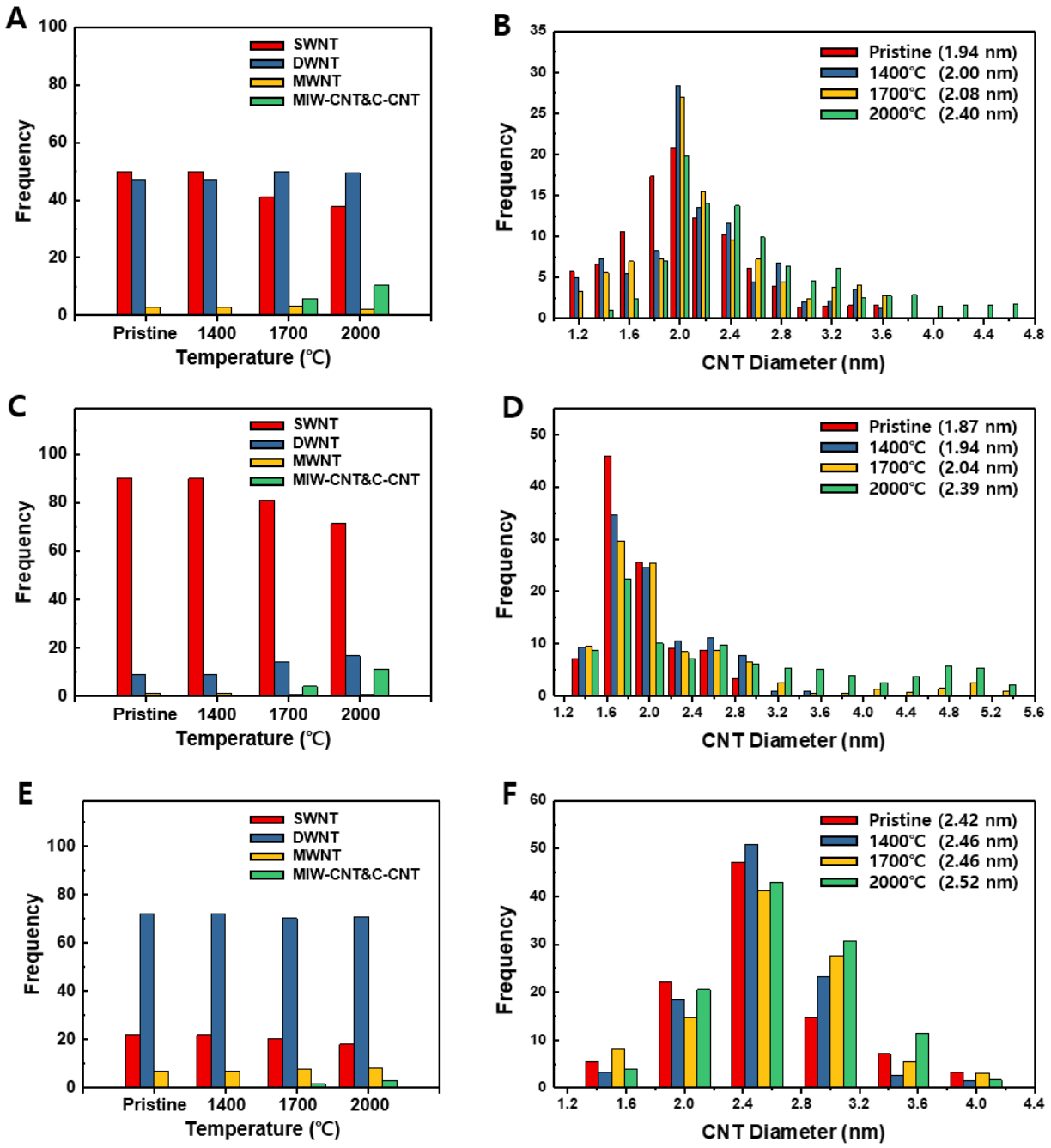

Figure S2. Distribution of diameters and number of walls distribution measured by analysis of TEM images after various thermal post-treatments. (**A** and **B**) CNT fibers with S·DWNT bundles, (**C** and **D**) SWNT bundles and (**E** and **F**) DWNT bundles.

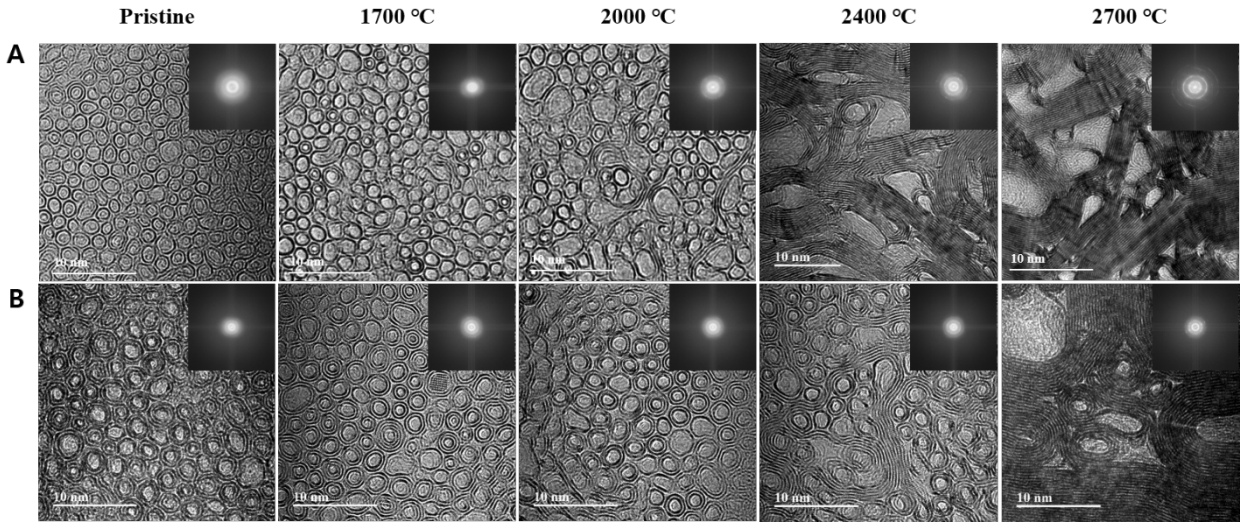

Figure S3. TEM image and diffraction pattern of CNT fibers. (**A**) CNT fibers with SWNT bundles and (**B**) DWNT bundles.

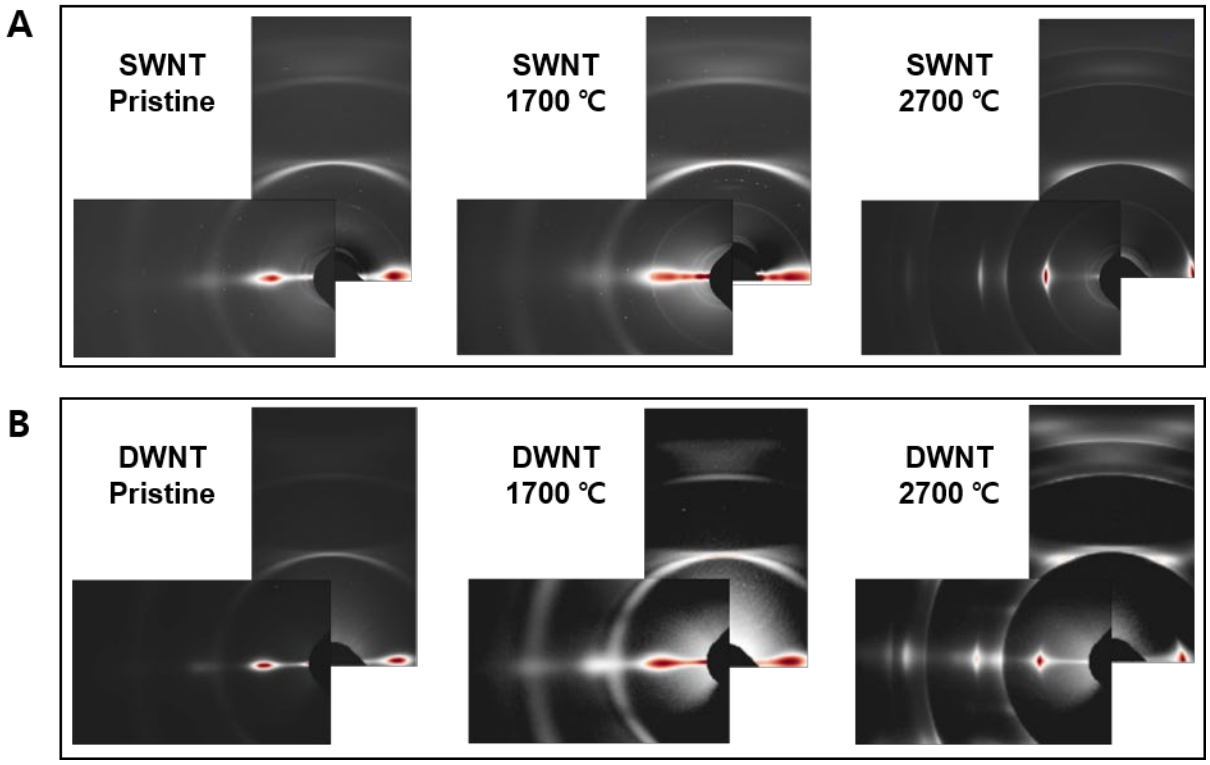

Figure S4. 2D WAXS patterns for CNT fibers. (**A**) SWNT fibers and (**B**) DWNT fibers, respectively, in pristine form and annealed at different temperatures.

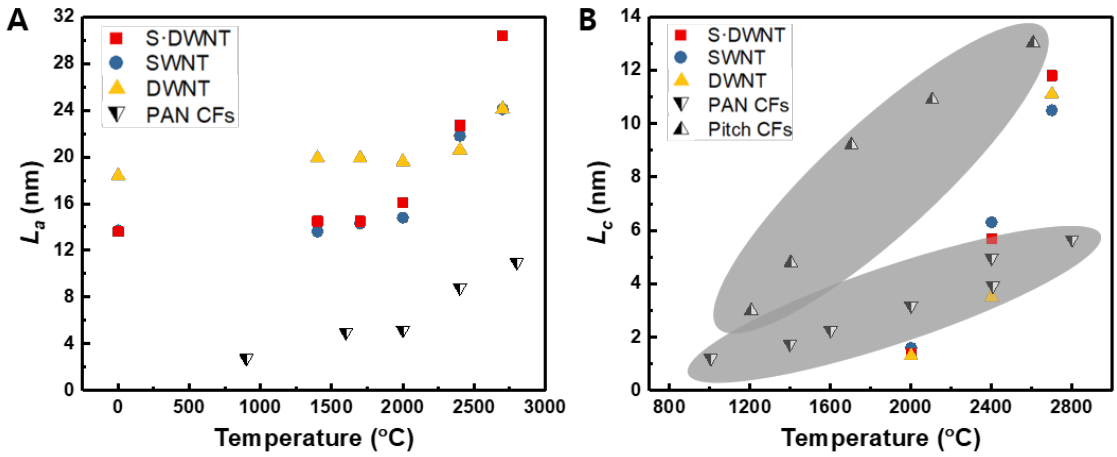

Figure S5. Changes in crystal size for pristine CNT fibers and annealed at different temperatures, including CFs for reference. Changes in (**A**) L_a and (**B**) L_c at each temperatures

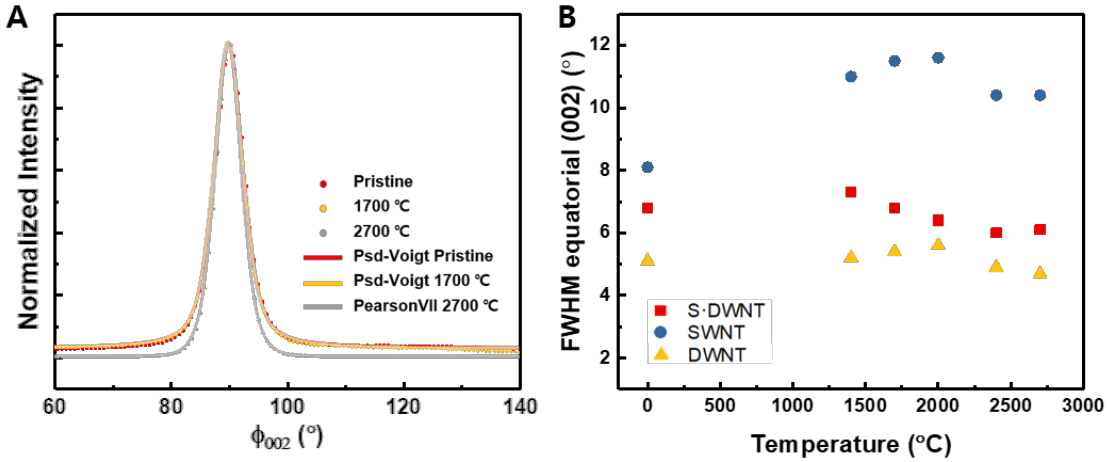

Figure S6. Changes in azimuthal FWHM and $\langle cos^2(\phi)\rangle$, for pristine CNT fibers and annealed at different temperatures. (**A**) Annealing increases the degree of alignment and changes the lineshape of the azimuthal profile at the tails of the distribution with a pronounced effect on $\langle cos^2(\phi)\rangle$. (**B**) Comparison of FWHM and of $\langle cos^2(\phi)\rangle$.

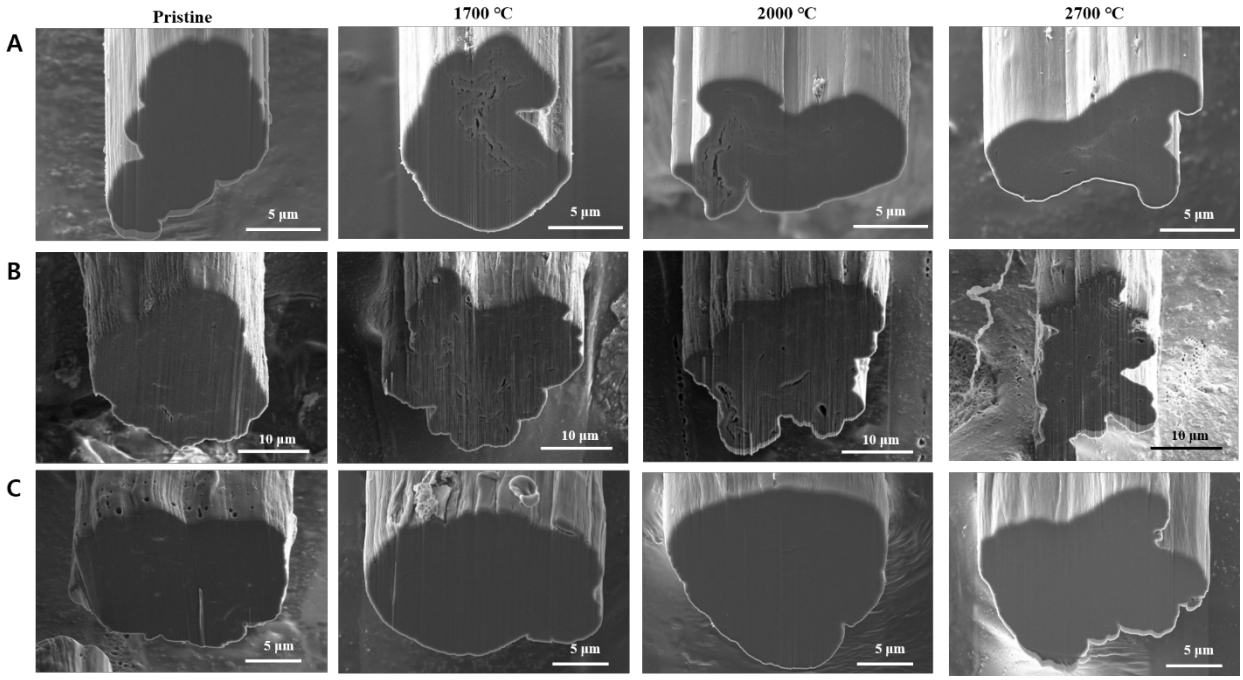

Figure S7. Cross-sectional SEM images of the CNT fibers. (**A**) S·DWNT fibers, (**B**) SWNT fibers and (**C**) DWNT fibers at each temperature.

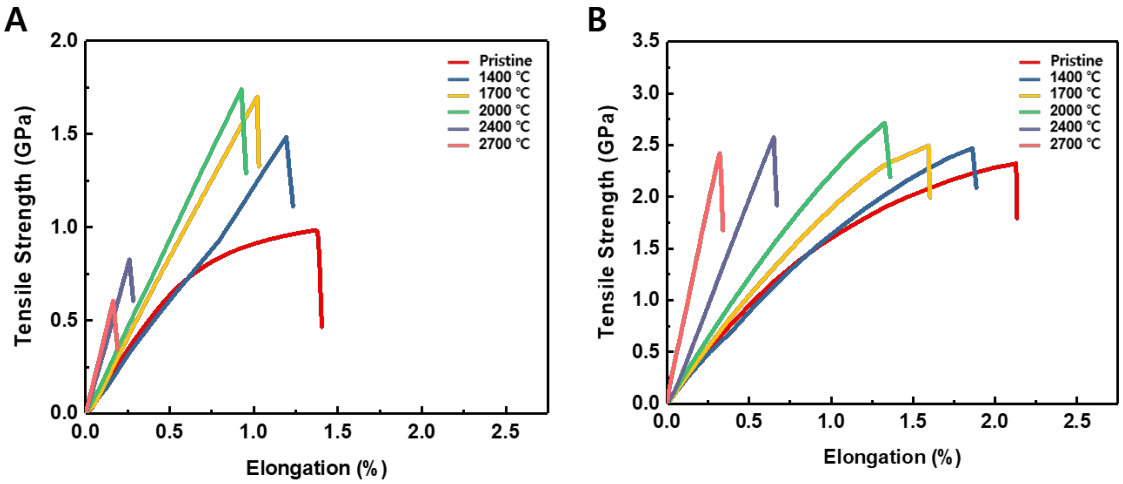

Figure S8. Stress-strain curves of CNT fibers. (**A**) SWNT fibers and (**B**) DWNT fibers.

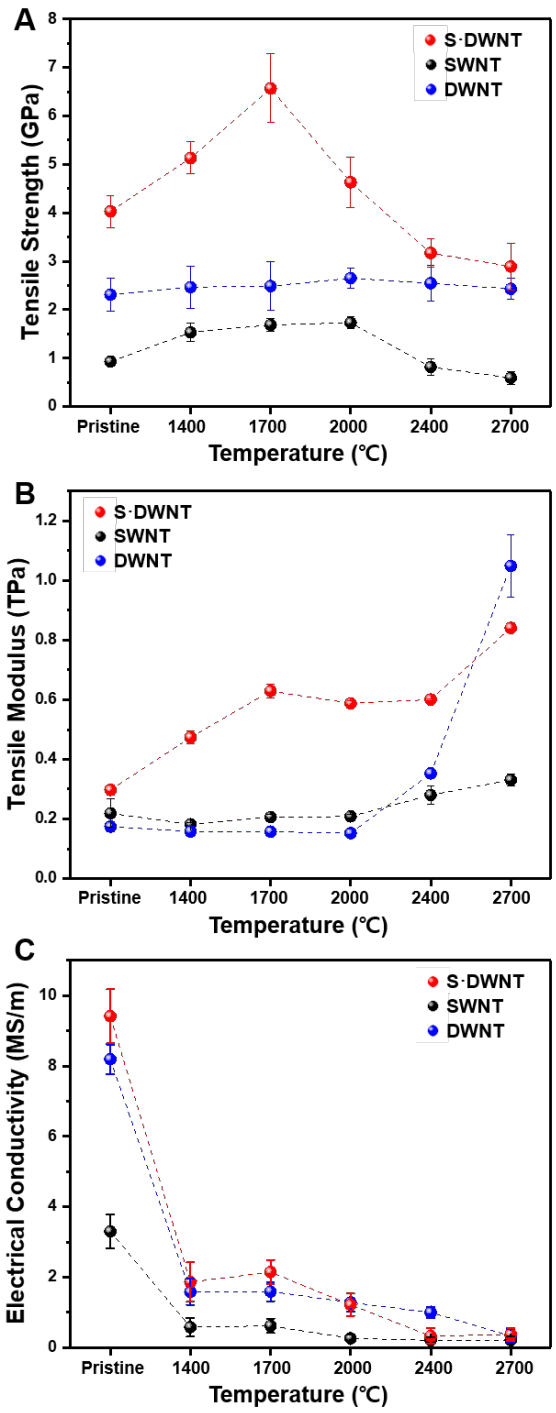

Figure S9. Mechanical and electrical properties of CNT fibers. (**A**) Tensile strength, (**B**) tensile modulus, and (**C**) room-temperature electrical conductivity of various CNT fibers as a function of annealing temperature.

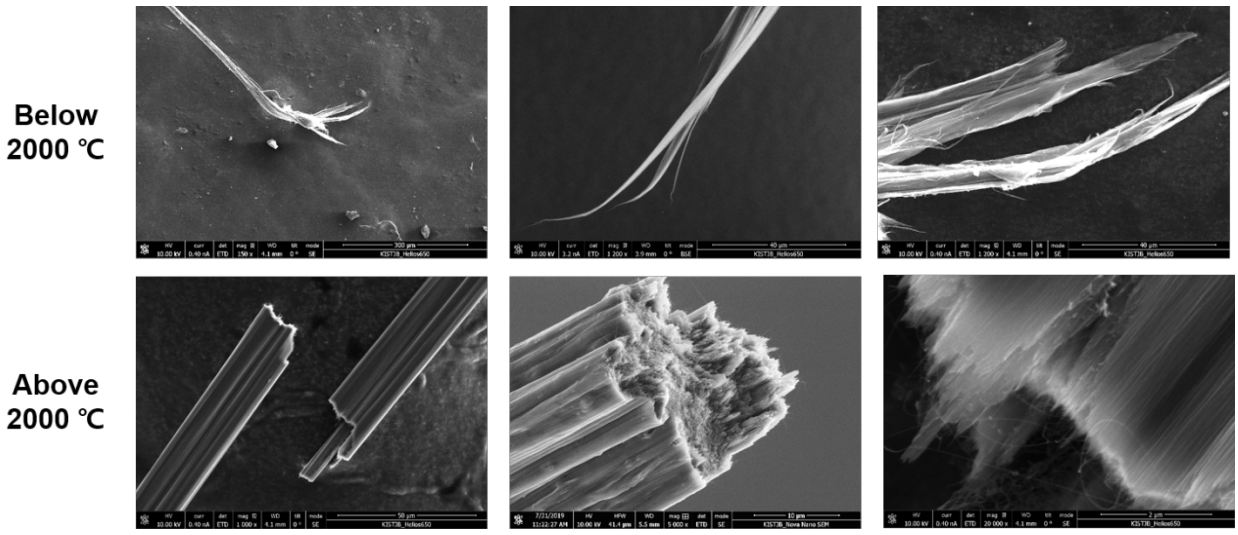

Figure S10. Fractography images of CNT fibers.

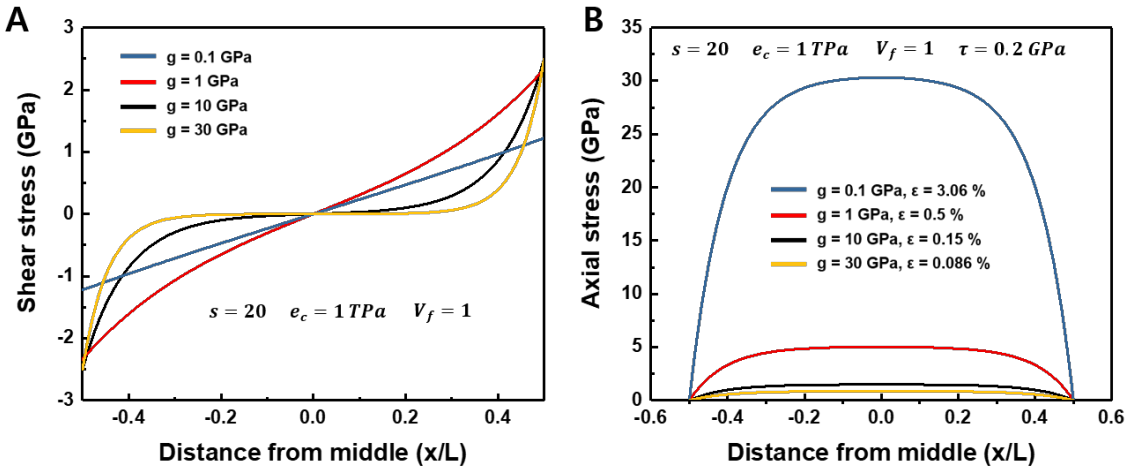

Figure S11. Calculated distributions of an idealized bundle. (**A**) shear stress and (**B**) maximum axial stress of an idealized bundle, for different values of shear modulus.

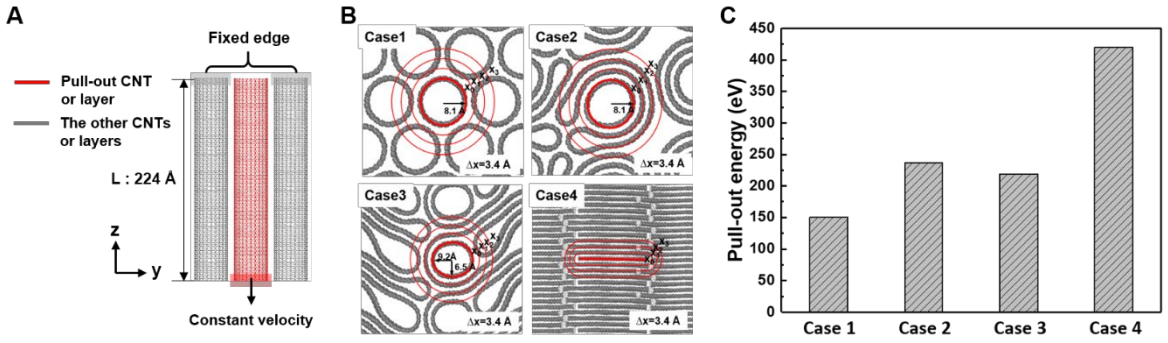

Figure S12. Shear strength between various CNTs by periodic boundary condition model. (A) Schematic of side view of CNT models. (**B**) Number of atoms vs distance graph of various CNT models. Cross-sectional Case1 simulates SWNT bundles, Case2 simulates SWNT wrapped with collapsed SWNT, Case3 simulates multi inner wall DWNT and Case4 simulates graphitic structure. The results on the pull-out simulation of the four different models after equilibration process: (**C**) the pull-out energy of the CNTs bundle and graphitic sheets.

The four different models in MD simulations were constructed to describe the structure of the obtained CNT fiber in the experiments. Four different models were considered: (case1) a nine-(12,12) SWNTs bundle, (case2) a two-(12,12) SWNTs and two-(42,42) SWNTs bundle, (case3) a one-(12,12) SWNT and one-(96,96) SWNT bundle, and (case4) a four-(12,12) layers and four-(15,15) layers bundle. The number of carbon atoms and the length of the bundle in all four models are 40176 and 224 Å, respectively. In order to stabilize the four models, the equilibration process was performed in three steps: (1) a 1 ns canonical (NVT) ensemble, (2) a 1 ns isothermal-isobaric (NPT) ensemble with a pressure of 1 atm, and (3) a 500 ps NVT ensemble. The time step and the temperature of the equilibration process were 1.0 fs and 300 K, respectively. A SWNT or layer of chirality (12,12) with a length of 224 Å in all four models was pulled out with a constant velocity of 0.1 Å/ps along the z direction after equilibration process. Every MD simulation was performed using the Adaptive Intermolecular Reactive Empirical Bond Order (AIREBO) potential, which has been widely used to describe the interaction between carbon atoms and predicted the mechanical properties of carbon materials (*47*).

The case1 was composed of the nine-(12,12) SWNTs bundle to describe the structure of the pristine CNT fiber obtained from the experimental data. Lopez et al. (*53*) studied the transformed structures of the CNTs bundle at high temperature using the MD simulation. They (*53*) reported that the coalescence of the CNTs bundle occurred due to the polymerization between CNTs and led to the cylindrical and collapsed CNT at high temperature. In this work, the two (42,42) SWNTs in the case2 were used as the coalesced tube from the (12,12) SWNTs for reducing the computational cost. Case2 shows that the (42,42) SWNT with a diameter of about 57 Å collapsed to the (12,12) SWNT with a diameter of about 16 Å. The (42,42) SWNT existed around the (12,12) SWNT along radial direction of CNT. The collapsed deformation between two CNTs with different diameters occurred due to the inner van der Waals attraction of CNT (*54*). The (96,96) SWNT with the largest diameter in the case3 was used as the coalesced tube from the two (42,42) SWNTs. The (96,96) SWNT collapsed to the (12,12) SWNT and was stacked by the strong van der Waals interaction. In the case4, the graphitic structure consists of the eight graphene layers in the periodic boundary conditions.

fig. S11C shows the potential energy for pulling the SWNT or layer from stabilized models. Each simulation model represented SWNT bundles (case1), SWNT wrapped with collapsed SWNT representing C-CNT (case2), MIW-DWNT representing MIW-CNT (case3) and GNR structure (case4). The case2 and case3 showed 58% and 46% higher pull-out energy than that of the case1. These results are related the number of atoms from the radius of the pull-out CNT to cut-off distance of 10.2 Å (fig. S11). In the case2, a lot of atoms were located around the pull-out CNT because the (42,42) SWNT with a large diameter collapsed to the pull-out CNT by the radial deformation. These results mean that the interfacial interaction was increased because the collapsed structure between the pull-out CNT and the other CNTs has the large contact area. In addition, the collapsed structure led to the strong van der Waals interaction. In comparison with the case2, the case3 had a smaller number of neighbor atoms around the pull-out CNT due to the presence of voids. The voids between tubes were caused by the coincidence of the cylindrical CNT and stacked graphitic shell. For that reason, the pull-out energy in the case3 was slightly decreased by the weak interfacial interaction between the pull-out CNT and graphitic shell. Among the four models, the pull-out layer in the case4 has the largest number of neighbor atoms within a cut-off

distance due to the graphitic structure of model. As the densely stacked layers induce the strongest interfacial interaction between pull-out layer and the other layers, the pull-out layer was pulled with the highest potential energy, which is 180% higher than that of the case1. These results suggest that the collapsed and graphitic structure are the crucial factors for the improvement of the mechanical property of the CNT fiber.

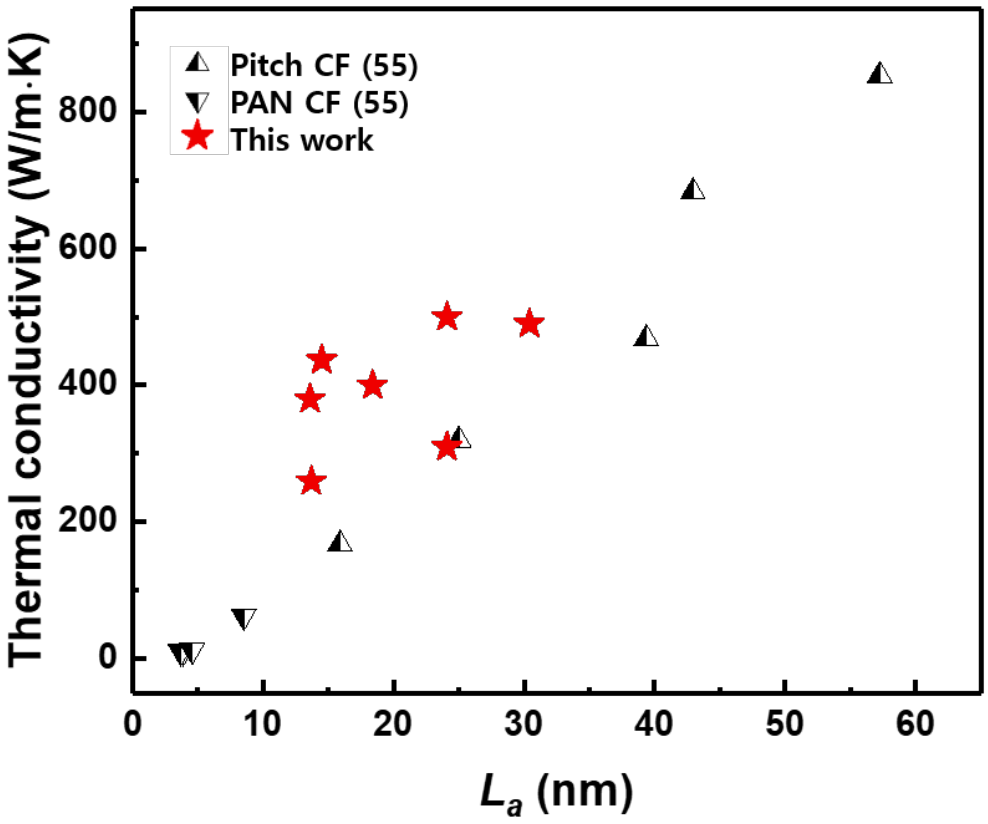

Figure S13. Thermal conductivity of CNT fibers and reference carbon fibers as a function of the L_a crystal size (*55*).

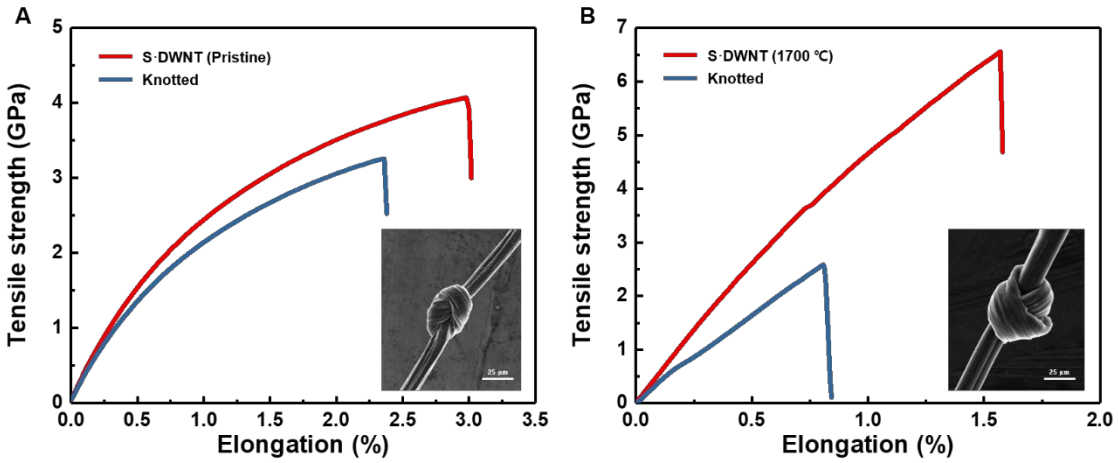

Figure S14. Knot efficiency of CNT fibers. (**A**) S·DWNT pristine fiber and (**B**) annealed fiber at 1700 °C.

Table S1. Average densities of CNT fibers measured by the density gradient column method and their tensile strength, modulus, electrical conductivity and thermal conductivity.

S-DWNT	Pristine	1400°C	1700°C	2000°C	2400°C	2700°C
Force (N)	0.53 ± 0.05	0.60 ± 0.05	0.73 ± 0.08	0.59 ± 0.07	0.42 ± 0.04	0.29 ± 0.05
Linear Density (tex)	0.25 ± 0.02	0.22 ± 0.03	0.19 ± 0.02	0.20 ± 0.02	0.19 ± 0.01	0.19 ± 0.01
Density (g/cm^3)	1.92	1.88	1.71	1.58	1.43	1.89
Specific Strength (N/tex)	2.10 ± 0.17	2.74 ± 0.18	3.84 ± 0.42	2.93 ± 0.33	2.22 ± 0.20	1.53 ± 0.26
Tensile Strength (GPa)	4.03 ± 0.33	5.13 ± 0.34	6.57 ± 0.72	4.63 ± 0.52	3.17 ± 0.29	2.89 ± 0.49
Specific Modulus (N/tex)	155 ± 9	252 ± 12	368 ± 13	372 ± 5	420 ± 2	445 ± 9.5
Tensile Modulus (GPa)	298 ± 17.28	474 ± 22.56	629 ± 22.23	588 ± 7.90	601 ± 2.86	841 ± 17.96
Elongation (%)	2.55 ± 0.37	1.82 ± 0.16	1.53 ± 0.21	1.15 ± 0.26	0.50 ± 0.17	0.36 ± 0.03
Specific Electrical Conductivity ($S·m^2/kg$)	5,200 ± 400	990 ± 300	1,300 ± 200	770 ± 200	230 ± 150	200 ± 100
Electrical Conductivity (MS/m)	10.88 ± 0.77	1.86 ± 0.56	2.22 ± 0.34	1.22 ± 0.32	0.33 ± 0.21	0.38 ± 0.19
Thermal Conductivity (W/m·K)	380 ± 21.46	N/A	482 ± 63.21	N/A	N/A	490 ± 31.67
SWNT	**Pristine**	**1400°C**	**1700°C**	**2000°C**	**2400°C**	**2700°C**
Force (N)	0.40 ± 0.04	0.67 ± 0.13	0.68 ± 0.05	0.71 ± 0.05	0.27 ± 0.08	0.18 ± 0.07
Linear Density (tex)	0.65 ± 0.01	0.60 ± 0.01	0.54 ± 0.01	0.54 ± 0.01	0.54 ± 0.01	0.54 ± 0.01
Density (g/cm^3)	1.6	1.32	1.35	1.32	1.63	1.80
Specific Strength (N/tex)	0.62 ± 0.06	1.12 ± 0.14	1.25 ± 0.10	1.32 ± 0.09	0.50 ± 0.11	0.34 ± 0.07
Tensile Strength (GPa)	0.98 ± 0.10	1.48 ± 0.18	1.69 ± 0.14	1.74 ± 0.12	0.81 ± 0.18	0.60 ± 0.13
Specific Modulus (N/tex)	137 ± 30	138 ± 5	153 ± 6	158 ± 6	172 ± 18	184 ± 11
Tensile Modulus (GPa)	219 ± 48.00	182 ± 6.60	207 ± 8.10	209 ± 7.92	280 ± 29.34	331 ± 19.80
Elongation (%)	1.31 ± 0.18	1.04 ± 0.21	1.18 ± 0.05	0.94 ± 0.09	0.28 ± 0.05	0.18 ± 0.07
Specific Electrical Conductivity ($S·m^2/kg$)	2,200 ± 300	440 ± 200	460 ± 150	200 ± 150	130 ± 100	120 ± 100
Electrical Conductivity (MS/m)	3.52 ± 0.48	0.58 ± 0.26	0.62 ± 0.20	0.26 ± 0.20	0.21 ± 0.16	0.22 ± 0.18
Thermal Conductivity (W/m·K)	213 ± 42.87	N/A	N/A	N/A	N/A	305 ± 5.23
DWNT	**Pristine**	**1400°C**	**1700°C**	**2000°C**	**2400°C**	**2700°C**
Force (N)	0.54 ± 0.07	0.56 ± 0.10	0.60 ± 0.12	0.65 ± 0.06	0.67 ± 0.07	0.46 ± 0.03
Linear Density (tex)	0.49 ± 0.02	0.42 ± 0.03	0.43 ± 0.02	0.41 ± 0.02	0.39 ± 0.03	0.37 ± 0.02
Density (g/cm^3)	2.10	1.84	1.79	1.71	1.61	1.96
Specific Strength (N/tex)	1.10 ± 0.16	1.34 ± 0.24	1.39 ± 0.28	1.59 ± 0.12	1.58 ± 0.23	1.24 ± 0.11
Tensile Strength (GPa)	2.31 ± 0.34	2.47 ± 0.44	2.49 ± 0.50	2.71 ± 0.21	2.54 ± 0.37	2.43 ± 0.22
Specific Modulus (N/tex)	83 ± 8	86 ± 9	88 ± 9	89 ±8	219 ± 11	535 ± 54
Tensile Modulus (GPa)	174 ± 16.80	158 ± 16.56	158 ± 16.11	152 ± 13.68	353 ± 17.71	1,049 ± 105.84
Elongation (%)	2.04 ± 0.38	1.67 ± 0.35	1.59 ± 0.05	1.33 ± 0.17	0.43 ± 0.12	0.33 ± 0.01
Specific Electrical Conductivity ($S·m^2/kg$)	3,900 ± 200	860 ± 200	890 ± 150	750 ± 150	620 ± 100	170 ± 100
Electrical Conductivity (MS/m)	8.19 ± 0.42	1.58 ± 0.37	1.59 ± 0.27	1.28 ± 0.26	1.00 ± 0.16	0.33 ± 0.20
Thermal Conductivity (W/m·K)	406 ± 8.69	N/A	N/A	N/A	N/A	496 ± 5.82

Table S2. Toughness and knot efficiency of S·DWNT fibers and CFs.

	S·DWNT (Pristine)	S·DWNT (1,400°C)	S·DWNT (1,700°C)	S·DWNT (2,000°C)	S·DWNT (2,400°C)	S·DWNT (2,700°C)	CF (T700)	CF (K13D2U)
Toughness (J/g)	39.38 ± 6.69	29.08 ± 4.94	33.76 ± 7.09	17.55 ± 5.18	5.59 ± 1.03	3.18 ± 0.46	27.85 ± 3.01	3.36 ± 0.42
Knot efficiency (%)	85 ± 5.09	61 ± 5.33	45 ± 8.27	17 ± 10.42	0	0	2.2 ± 1.0	0

REFERENCES AND NOTES

1. H. G. Chae, S. Kumar, Making strong fibers. *Science* **319**, 908–909 (2008).

2. C. Lee, X. Wei, J. W. Kysar, J. Hone, Measurement of the elastic properties and intrinsic strength of monolayer graphene. *Science* **321**, 385–388 (2008).

3. A. Javey, J. Guo, Q. Wang, M. Lundstrom, H. Dai, Ballistic carbon nanotube field-effect transistors. *Nature* **424**, 654–657 (2003).

4. C. Yu, L. Shi, Z. Yao, D. Li, A. Majumdar, Thermal conductance and thermopower of an individual single-wall carbon nanotube. *Nano Lett.* **5**, 1842–1846 (2005).

5. M. Adnan, R. A. Pinnick, Z. Tang, L. W. Taylor, S. S. Pamulapati, G. R. Carfagni, M. Pasquali, Bending behavior of CNT fibers and their scaling laws. *Soft Matter* **14**, 8284–8292 (2018).

6. M. Miao, *Carbon Nanotube Fibres and Yarns: Production, Properties and Applications in Smart Textiles* (Elsevier, Cambridge, 2019).

7. L. W. Taylor, O. S. Dewey, R. J. Headrick, N. Komatsu, N. M. Peraca, G. Wehmeyer, J. Kono, M. Pasquali, Improved properties, increased production, and the path to broad adoption of carbon nanotube fibers. *Carbon* **171**, 689–694 (2021).

8. N. Gupta, J. M. Alred, E. S. Penev, B. I. Yakobson, Universal strength scaling in carbon nanotube bundles with frictional load transfer. *ACS Nano* **15**, 1342–1350 (2021).

9. X. Zhang, W. Lu, G. Zhou, Q. Li, Understanding the mechanical and conductive properties of carbon nanotube fibers for smart electronics. *Adv. Mater.* **32**, 1902028 (2020).

10. N. Behabtu, C. C. Young, D. E. Tsentalovich, O. Kleinerman, X. Wang, A. W. K. Ma, E. A. Bengio, R. F. ter Waarbeek, J. J. de Jong, R. E. Hoogerwerf, S. B. Fairchild, J. B. Ferguson, B. Maruyama, J. Kono, Y. Talmon, Y. Cohen, M. J. Otto, M. Pasquali, Strong, light, multifunctional fibers of carbon nanotubes with ultrahigh conductivity. *Science* **339**, 182–186 (2013).

11. J. J. Vilatela, J. A. Elliott, A. H. Windle, A model for the strength of yarn-like carbon nanotube fibers. *ACS Nano* **5**, 1921–1927 (2011).

12. B. D. Jensen, J.-W. Kim, G. Sauti, K. E. Wise, L. Dong, H. N. G. Wadley, J. G. Park, R. Liang, E. J. Siochi, Toward ultralight high-strength structural materials via collapsed carbon nanotube bonding. *Carbon* **156**, 538–548 (2020).

13. D. Qian, W. K. Liu, R. S. Ruoff, Load transfer mechanism in carbon nanotube ropes. *Compos. Sci. Technol.* **63**, 1561–1569 (2003).

14. M. Terrones, H. Terrones, F. Banhart, J.-C. Charlier, P. M. Ajayan, Coalescence of single-walled carbon nanotubes. *Science* **288**, 1226–1229 (2000).

15. J. A. Elliott, J. K. W. Sandler, A. H. Windle, R. J. Young, M. S. P. Shaffer, Collapse of single-wall carbon nanotubes is diameter dependent. *Phys. Rev. Lett.* **92**, 095501 (2004).

16. U. J. Kim, H. R. Gutiérrez, J. P. Kim, P. C. Eklund, Effect of the tube diameter distribution on the high-temperature structural modification of bundled single-walled carbon nanotubes. *J. Phys. Chem. B* **109**, 23358–23365 (2005).

17. M. J. López, A. Rubio, J. A. Alonso, S. Lefrant, K. Méténier, S. Bonnamy, Patching and tearing single-wall carbon-nanotube ropes into multiwall carbon nanotubes. *Phys. Rev. Lett.* **89**, 255501 (2002).

18. H. D. Jeong, S. G. Kim, G. M. Choi, M. Park, B.-C Ku, H. S. Lee, Theoretical and experimental investigation of the wet-spinning process for mechanically strong carbon nanotube fibers. *Chem. Eng. J.* **412**, 128650 (2021).

19. S. Jin, B. Chung, H. J. Park, B. V. Cunning, J.-H. Lee, A. Yoon, M. Huang, H. Seo, D. Lee, Z. Lee, R. S. Ruoff, S. Ryu, Ultrahigh strength and modulus graphene-based hybrid carbons with AB-stacked and turbostratic structures. *Adv. Funct. Mater.* **30**, 2005381 (2020).

20. D. D. L. Chung, *Carbon Composites: Composites with Carbon Fibers, Nanofibers, and Nanotubes* (Elsevier, Cambridge, 2016).

21. H. J. C. Berendsen, J. P. M. Postma, W. F. van Gunsteren, A. Dinola, J. R. Haak, Molecular dynamics with coupling to an external bath. *J. Chem. Phys.* **81**, 3684-3690 (1984).

22. M. G. Northolt, P. den Decker, S. J. Picken, J. J. M. Baltussen, R. Schlatmann, The Tensile strength of polymer fibres. *Adv. Polym. Sci.* **178**, 1–108 (2005).

23. B. T. Kelly, *The Physics of Graphite* (Applied Science Publishers, 1981).

24. X. Wei, M. Ford, R. A. Soler-Crespo, H. D. Espinosa, A new Monte Carlo model for predicting the mechanical properties of fiber yarns. *J. Mech. Phys. Solids* **84**, 325–335 (2015).

25. H. N. Yoon, Strength of fibers from wholly aromatic polyesters. *Colloid Polym. Sci.* **268**, 230–239 (1990).

26. M. J. Behr, B. G. Landes, B. E. Barton, M. T. Bernius, G. F. Billovits, E. J. Hukkanen, J. T. Patton, W. Wang, C. Wood, D. T. Keane, J. E. Rix, S. J. Weigand, Structure-property model for polyethylene-derived carbon fiber. *Carbon* **107**, 525–535 (2016).

27. Y. Shibuta, J. A. Elliott, Interaction between two graphene sheets with a turbostratic orientational relationship. *Chem. Phys. Lett.* **512**, 146–150 (2011).

28. B. Kumanek, D. Janas, Thermal conductivity of carbon nanotube networks: A review. *J. Mater. Sci.* **54**, 7397–7427 (2019).

29. S. B. Fairchild, T. A. de Assis, J. H. Park, M. Cahay, J. Bulmer, D. E. Tsentalovich, Y. S. Ang, L. K. Ang, J. Ludwick, T. C. Back, M. Pasquali, Strongly anisotropic field emission from highly aligned carbon nanotube films. *J. Appl. Phys.* **129**, 125103 (2021).

30. D. E. Tsentalovich, R. J. Headrick, F. Mirri, J. Hao, N. Behabtu, C. C. Young, M. Pasquali, Influence of carbon nanotube characteristics on macroscopic fiber properties. *ACS Appl. Mater. Interfaces* **9**, 36189–36198 (2017).

31. F. Hao, D. Fang, Z. Xu, Mechanical and thermal transport properties of graphene with defects. *Appl. Phys. Lett.* **99**, 041901 (2011).

32. G. Xie, Y. Shen, X. Wei, L. Yang, H. Xiao, J. Zhong, G. Zhang, A bond-order theory on the phonon scattering by vacancies in two-dimensional materials. *Sci. Rep.* **4**, 5085 (2014).

33. Z. G. Fthenakis, Z. Zhu, D. Tománek, Effect of structural defects on the thermal conductivity of graphene: From point to line defects to haeckelites. *Phys. Rev. B* **89**, 125421 (2014).

34. Y. Anno, Y. Imakita, K. Takei, S. Akita, T. Arie, Enhancement of graphene thermoelectric performance through defect engineering. *2D Mater.* **4**, 025019 (2017).

35. P. Yasaei, A. Fathizadeh, R. Hantehzadeh, A. K. Majee, A. El-Ghandour, D. Estrada, C. Foster, Z. Aksamija, F. Khalili-Araghi, A. Salehi-Khojin, Bimodal phonon scattering in graphene grain boundaries. *Nano Lett.* **15**, 4532–4540 (2015).

36. H. K. Liu, Y. Lin, S. N. Luo, Grain boundary energy and grain size dependences of thermal conductivity of polycrystalline graphene. *J. Phys. Chem. C* **118**, 24797–24802 (2014).

37. L. Qiu, X. Zhang, Z. Guo, Q. Li, Interfacial heat transport in nano-carbon assemblies. *Carbon* **178**, 391–412 (2021).

38. V. A. Davis, L. M. Ericson, A. N. G. Parra-Vasquez, H. Fan, Y. Wang, V. Prieto, J. A. Longoria, S. Ramesh, R. K. Saini, C. Kittrell, W. E. Billups, W. W. Adams, R. H. Hauge, R. E. Smalley, M. Pasquali, Phase behavior and rheology of SWNTs in superacids. *Macromolecules* **37**, 154–160 (2004).

39. V. Datsyuk, M. Kalyva, K. Papagelis, J. Parthenios, D. Tasis, A. Siokou, I. Kallitsis, C. Galiotis, Chemical oxidation of multiwalled carbon nanotubes. *Carbon* **46**, 833–840 (2008).

40. J. Park, S.-H. Lee, J. Lee, D.-M. Lee, H. Yu, H. S. Jeong, S. M. Kim, K.-H. Lee, Accurate measurement of specific tensile strength of carbon nanotube fibers with hierarchical structures by vibroscopic method. *RSC Adv.* **7**, 8575–8580 (2017).

41. A. Milev, M. Wilson, G. S. K. Kannangara, N. Tran, X-ray diffraction line profile analysis of nanocrystalline graphite. *Mater. Chem. Phys.* **111**, 346–350 (2008).

42. W. Ruland, B. Smarsly, X-ray scattering of non-graphitic carbon: An improved method of evaluation. *J. Appl. Cryst.* **35**, 624–633 (2002).

43. G. A. Zickler, B. Smarsly, N. Gierlinger, H. Peterlik, O. Paris, A reconsideration of the relationship between the crystallite size L_a of carbons determined by X-ray diffraction and Raman spectroscopy. *Carbon* **44**, 3239–3246 (2006).

44. J. Moon, K. Weaver, B. Feng, H. G. Chae, S. Kumar, J.-B. Baek, G. P. Peterson, Note: Thermal conductivity measurement of individual poly(ether ketone)/carbon nanotube fibers using a steady-state dc thermal bridge method. *Rev. Sci. Instrum.* **83**, 016103 (2012).

45. L. Qiu, X. Wang, D. Tang, X. Zheng, P. M. Norris, D. Wen, J. Zhao, X. Zhang, Q. Li, Functionalization and densification of inter-bundle interfaces for improvement in electrical and thermal transport of carbon nanotube fibers. *Carbon* **105**, 248–259 (2016).

46. S. Izrailev, S. Stepaniants, B. Isralewitz, D. Kosztin, H. Lu, F. Molnar, W. Wriggers, K. Schulten, *Steered Molecular Dynamics, Computational Molecular Dynamics: Challenges, Methods, Ideas* (Springer, 1998), pp. 39–65.

47. S. Park, K. Schulten, Calculating potentials of mean force from steered molecular dynamics simulations. *J. Chem. Phys.* **120**, 5946–5961 (2004).

48. A. Takaku, M. Shioya, X-ray measurements and the structure of polyacrylonitrile- and pitch-based carbon fibres. *J. Mater. Sci.* **25**, 4873–4879 (1990).

49. J. Lee, D.-M. Lee, Y. Jung, J. Park, H. S. Lee, Y.-K. Kim, C. R. Park, H. S. Jeong, S. M. Kim, Direct spinning and densification method for high-performance carbon nanotube fibers. *Nat. Commun.* **10**, 2962 (2019).

50. T. Q. Tran, Z. Fan, P. Liu, S. M. Myint, H. M. Duong, Super-strong and highly conductive carbon nanotube ribbons from post-treatment methods. *Carbon* **99**, 407–415 (2016).

51. J. N. Wang, X. G. Luo, T. Wu, Y. Chen, High-strength carbon nanotube fibre-like ribbon with high ductility and high electrical conductivity. *Nat. Commun.* **5**, 3848 (2014).

52. G. Xin, T. Yao, H. Sun, S. M. Scott, D. Shao, G. Wang, J. Lian, Highly thermally conductive and mechanically strong graphene fibers. *Science*, **349**, 1083–1087 (2015).

53. S. J. Stuart, A. B. Tutein, J. A. Harrison, A reactive potential for hydrocarbons with intermolecular interactions. *J. Chem. Phys.* **112**, 6472–6486 (2000).

54. X. Yuan, Y. Wang, B. Zhu, Adhesion between two carbon nanotubes: Insights from molecular dynamics simulations and continuum mechanics. *Int. J. Mech. Sci.* **138-139**, 323–336 (2018).

55. D. Jang, S. Lee, Correlating thermal conductivity of carbon fibers with mechanical and structural properties. *J. Ind. Eng. Chem.* **89**, 115–118 (2020).

REFERENCES AND NOTES

1. H. G. Chae, S. Kumar, Making strong fibers. *Science* **319**, 908–909 (2008).

2. C. Lee, X. Wei, J. W. Kysar, J. Hone, Measurement of the elastic properties and intrinsic strength of monolayer graphene. *Science* **321**, 385–388 (2008).

3. A. Javey, J. Guo, Q. Wang, M. Lundstrom, H. Dai, Ballistic carbon nanotube field-effect transistors. *Nature* **424**, 654–657 (2003).

4. C. Yu, L. Shi, Z. Yao, D. Li, A. Majumdar, Thermal conductance and thermopower of an individual single-wall carbon nanotube. *Nano Lett.* **5**, 1842–1846 (2005).

5. M. Adnan, R. A. Pinnick, Z. Tang, L. W. Taylor, S. S. Pamulapati, G. R. Carfagni, M. Pasquali, Bending behavior of CNT fibers and their scaling laws. *Soft Matter* **14**, 8284–8292 (2018).

6. M. Miao, *Carbon Nanotube Fibres and Yarns: Production, Properties and Applications in Smart Textiles* (Elsevier, Cambridge, 2019).

7. L. W. Taylor, O. S. Dewey, R. J. Headrick, N. Komatsu, N. M. Peraca, G. Wehmeyer, J. Kono, M. Pasquali, Improved properties, increased production, and the path to broad adoption of carbon nanotube fibers. *Carbon* **171**, 689–694 (2021).

8. N. Gupta, J. M. Alred, E. S. Penev, B. I. Yakobson, Universal strength scaling in carbon nanotube bundles with frictional load transfer. *ACS Nano* **15**, 1342–1350 (2021).

9. X. Zhang, W. Lu, G. Zhou, Q. Li, Understanding the mechanical and conductive properties of carbon nanotube fibers for smart electronics. *Adv. Mater.* **32**, 1902028 (2020).

10. N. Behabtu, C. C. Young, D. E. Tsentalovich, O. Kleinerman, X. Wang, A. W. K. Ma, E. A. Bengio, R. F. ter Waarbeek, J. J. de Jong, R. E. Hoogerwerf, S. B. Fairchild, J. B. Ferguson, B. Maruyama, J. Kono, Y. Talmon, Y. Cohen, M. J. Otto, M. Pasquali, Strong, light, multifunctional fibers of carbon nanotubes with ultrahigh conductivity. *Science* **339**, 182–186 (2013).

11. J. J. Vilatela, J. A. Elliott, A. H. Windle, A model for the strength of yarn-like carbon nanotube fibers. *ACS Nano* **5**, 1921–1927 (2011).

12. B. D. Jensen, J.-W. Kim, G. Sauti, K. E. Wise, L. Dong, H. N. G. Wadley, J. G. Park, R. Liang, E. J. Siochi, Toward ultralight high-strength structural materials via collapsed carbon nanotube bonding. *Carbon* **156**, 538–548 (2020).

13. D. Qian, W. K. Liu, R. S. Ruoff, Load transfer mechanism in carbon nanotube ropes. *Compos. Sci. Technol.* **63**, 1561–1569 (2003).

14. M. Terrones, H. Terrones, F. Banhart, J.-C. Charlier, P. M. Ajayan, Coalescence of single-walled carbon nanotubes. *Science* **288**, 1226–1229 (2000).

15. J. A. Elliott, J. K. W. Sandler, A. H. Windle, R. J. Young, M. S. P. Shaffer, Collapse of single-wall carbon nanotubes is diameter dependent. *Phys. Rev. Lett.* **92**, 095501 (2004).

16. U. J. Kim, H. R. Gutiérrez, J. P. Kim, P. C. Eklund, Effect of the tube diameter distribution on the high-temperature structural modification of bundled single-walled carbon nanotubes. *J. Phys. Chem. B* **109**, 23358–23365 (2005).

17. M. J. López, A. Rubio, J. A. Alonso, S. Lefrant, K. Méténier, S. Bonnamy, Patching and tearing single-wall carbon-nanotube ropes into multiwall carbon nanotubes. *Phys. Rev. Lett.* **89**, 255501 (2002).

18. H. D. Jeong, S. G. Kim, G. M. Choi, M. Park, B.-C Ku, H. S. Lee, Theoretical and experimental investigation of the wet-spinning process for mechanically strong carbon nanotube fibers. *Chem. Eng. J.* **412**, 128650 (2021).

19. S. Jin, B. Chung, H. J. Park, B. V. Cunning, J.-H. Lee, A. Yoon, M. Huang, H. Seo, D. Lee, Z. Lee, R. S. Ruoff, S. Ryu, Ultrahigh strength and modulus graphene-based hybrid carbons with AB-stacked and turbostratic structures. *Adv. Funct. Mater.* **30**, 2005381 (2020).

20. D. D. L. Chung, *Carbon Composites: Composites with Carbon Fibers, Nanofibers, and Nanotubes* (Elsevier, Cambridge, 2016).

21. H. J. C. Berendsen, J. P. M. Postma, W. F. van Gunsteren, A. Dinola, J. R. Haak, Molecular dynamics with coupling to an external bath. *J. Chem. Phys.* **81**, 3684-3690 (1984).

22. M. G. Northolt, P. den Decker, S. J. Picken, J. J. M. Baltussen, R. Schlatmann, The Tensile strength of polymer fibres. *Adv. Polym. Sci.* **178**, 1–108 (2005).

23. B. T. Kelly, *The Physics of Graphite* (Applied Science Publishers, 1981).

24. X. Wei, M. Ford, R. A. Soler-Crespo, H. D. Espinosa, A new Monte Carlo model for predicting the mechanical properties of fiber yarns. *J. Mech. Phys. Solids* **84**, 325–335 (2015).

25. H. N. Yoon, Strength of fibers from wholly aromatic polyesters. *Colloid Polym. Sci.* **268**, 230–239 (1990).

26. M. J. Behr, B. G. Landes, B. E. Barton, M. T. Bernius, G. F. Billovits, E. J. Hukkanen, J. T. Patton, W. Wang, C. Wood, D. T. Keane, J. E. Rix, S. J. Weigand, Structure-property model for polyethylene-derived carbon fiber. *Carbon* **107**, 525–535 (2016).

27. Y. Shibuta, J. A. Elliott, Interaction between two graphene sheets with a turbostratic orientational relationship. *Chem. Phys. Lett.* **512**, 146–150 (2011).

28. B. Kumanek, D. Janas, Thermal conductivity of carbon nanotube networks: A review. *J. Mater. Sci.* **54**, 7397–7427 (2019).

29. S. B. Fairchild, T. A. de Assis, J. H. Park, M. Cahay, J. Bulmer, D. E. Tsentalovich, Y. S. Ang, L. K. Ang, J. Ludwick, T. C. Back, M. Pasquali, Strongly anisotropic field emission from highly aligned carbon nanotube films. *J. Appl. Phys.* **129**, 125103 (2021).

30. D. E. Tsentalovich, R. J. Headrick, F. Mirri, J. Hao, N. Behabtu, C. C. Young, M. Pasquali, Influence of carbon nanotube characteristics on macroscopic fiber properties. *ACS Appl. Mater. Interfaces* **9**, 36189–36198 (2017).

31. F. Hao, D. Fang, Z. Xu, Mechanical and thermal transport properties of graphene with defects. *Appl. Phys. Lett.* **99**, 041901 (2011).

32. G. Xie, Y. Shen, X. Wei, L. Yang, H. Xiao, J. Zhong, G. Zhang, A bond-order theory on the phonon scattering by vacancies in two-dimensional materials. *Sci. Rep.* **4**, 5085 (2014).

33. Z. G. Fthenakis, Z. Zhu, D. Tománek, Effect of structural defects on the thermal conductivity of graphene: From point to line defects to haeckelites. *Phys. Rev. B* **89**, 125421 (2014).

34. Y. Anno, Y. Imakita, K. Takei, S. Akita, T. Arie, Enhancement of graphene thermoelectric performance through defect engineering. *2D Mater.* **4**, 025019 (2017).

35. P. Yasaei, A. Fathizadeh, R. Hantehzadeh, A. K. Majee, A. El-Ghandour, D. Estrada, C. Foster, Z. Aksamija, F. Khalili-Araghi, A. Salehi-Khojin, Bimodal phonon scattering in graphene grain boundaries. *Nano Lett.* **15**, 4532–4540 (2015).

36. H. K. Liu, Y. Lin, S. N. Luo, Grain boundary energy and grain size dependences of thermal conductivity of polycrystalline graphene. *J. Phys. Chem. C* **118**, 24797–24802 (2014).

37. L. Qiu, X. Zhang, Z. Guo, Q. Li, Interfacial heat transport in nano-carbon assemblies. *Carbon* **178**, 391–412 (2021).

38. V. A. Davis, L. M. Ericson, A. N. G. Parra-Vasquez, H. Fan, Y. Wang, V. Prieto, J. A. Longoria, S. Ramesh, R. K. Saini, C. Kittrell, W. E. Billups, W. W. Adams, R. H. Hauge, R. E. Smalley, M. Pasquali, Phase behavior and rheology of SWNTs in superacids. *Macromolecules* **37**, 154–160 (2004).

39. V. Datsyuk, M. Kalyva, K. Papagelis, J. Parthenios, D. Tasis, A. Siokou, I. Kallitsis, C. Galiotis, Chemical oxidation of multiwalled carbon nanotubes. *Carbon* **46**, 833–840 (2008).

40. J. Park, S.-H. Lee, J. Lee, D.-M. Lee, H. Yu, H. S. Jeong, S. M. Kim, K.-H. Lee, Accurate measurement of specific tensile strength of carbon nanotube fibers with hierarchical structures by vibroscopic method. *RSC Adv.* **7**, 8575–8580 (2017).

41. A. Milev, M. Wilson, G. S. K. Kannangara, N. Tran, X-ray diffraction line profile analysis of nanocrystalline graphite. *Mater. Chem. Phys.* **111**, 346–350 (2008).

42. W. Ruland, B. Smarsly, X-ray scattering of non-graphitic carbon: An improved method of evaluation. *J. Appl. Cryst.* **35**, 624–633 (2002).

43. G. A. Zickler, B. Smarsly, N. Gierlinger, H. Peterlik, O. Paris, A reconsideration of the relationship between the crystallite size L_a of carbons determined by X-ray diffraction and Raman spectroscopy. *Carbon* **44**, 3239–3246 (2006).

44. J. Moon, K. Weaver, B. Feng, H. G. Chae, S. Kumar, J.-B. Baek, G. P. Peterson, Note: Thermal conductivity measurement of individual poly(ether ketone)/carbon nanotube fibers using a steady-state dc thermal bridge method. *Rev. Sci. Instrum.* **83**, 016103 (2012).

45. L. Qiu, X. Wang, D. Tang, X. Zheng, P. M. Norris, D. Wen, J. Zhao, X. Zhang, Q. Li, Functionalization and densification of inter-bundle interfaces for improvement in electrical and thermal transport of carbon nanotube fibers. *Carbon* **105**, 248–259 (2016).

46. S. Izrailev, S. Stepaniants, B. Isralewitz, D. Kosztin, H. Lu, F. Molnar, W. Wriggers, K. Schulten, *Steered Molecular Dynamics, Computational Molecular Dynamics: Challenges, Methods, Ideas* (Springer, 1998), pp. 39–65.

47. S. Park, K. Schulten, Calculating potentials of mean force from steered molecular dynamics simulations. *J. Chem. Phys.* **120**, 5946–5961 (2004).

48. A. Takaku, M. Shioya, X-ray measurements and the structure of polyacrylonitrile- and pitch-based carbon fibres. *J. Mater. Sci.* **25**, 4873–4879 (1990).

49. J. Lee, D.-M. Lee, Y. Jung, J. Park, H. S. Lee, Y.-K. Kim, C. R. Park, H. S. Jeong, S. M. Kim, Direct spinning and densification method for high-performance carbon nanotube fibers. *Nat. Commun.* **10**, 2962 (2019).

50. T. Q. Tran, Z. Fan, P. Liu, S. M. Myint, H. M. Duong, Super-strong and highly conductive carbon nanotube ribbons from post-treatment methods. *Carbon* **99**, 407–415 (2016).

51. J. N. Wang, X. G. Luo, T. Wu, Y. Chen, High-strength carbon nanotube fibre-like ribbon with high ductility and high electrical conductivity. *Nat. Commun.* **5**, 3848 (2014).

52. G. Xin, T. Yao, H. Sun, S. M. Scott, D. Shao, G. Wang, J. Lian, Highly thermally conductive and mechanically strong graphene fibers. *Science*, **349**, 1083–1087 (2015).

53. S. J. Stuart, A. B. Tutein, J. A. Harrison, A reactive potential for hydrocarbons with intermolecular interactions. *J. Chem. Phys.* **112**, 6472–6486 (2000).

54. X. Yuan, Y. Wang, B. Zhu, Adhesion between two carbon nanotubes: Insights from molecular dynamics simulations and continuum mechanics. *Int. J. Mech. Sci.* **138-139**, 323–336 (2018).

55. D. Jang, S. Lee, Correlating thermal conductivity of carbon fibers with mechanical and structural properties. *J. Ind. Eng. Chem.* **89**, 115–118 (2020).